PROTEINS: Structure, Function, and Genetics 42:182–191 (2001)

Three-dimensional Structure of a Complex of Galanthamine (Nivalin®) with Acetylcholinesterase From *Torpedo californica*: Implications for the Design of New Anti-Alzheimer Drugs

Cecilia Bartolucci,[1] , Emanuele Perola,[2] Christian Pilger,[3] Gregor Fels,[3] and Doriano Lamba[1,4*]
[1]*Istituto di Strutturistica Chimica "G. Giacomello," Monterotondo Stazione (Roma), Italy*
[2] *Department of Molecular Pharmacology and Experimental Therapeutics, Mayo Clinic and Mayo Foundation, Rochester, Minnesota*
[3]*Universität-GH Paderborn, Chemie und Chemietechnik, Paderborn, Germany*
[4]*International Centre for Genetic Engineering and Biotechnology, Area Science Park, Trieste, Italy*

ABSTRACT **The 3D structure of a complex of the anti-Alzheimer drug galanthamine with *Torpedo californica* acetylcholinesterase is reported. Galanthamine, a tertiary alkaloid extracted from several species of *Amarylidacae*, is so far the only drug that shows a dual activity, being both an acetylcholinesterase inhibitor and an allosteric potentiator of the nicotinic response induced by acetylcholine and competitive agonists. The X-ray structure, at 2.5Å resolution, shows an unexpected orientation of the ligand within the active site, as well as unusual protein–ligand interactions. The inhibitor binds at the base of the active site gorge, interacting with both the acyl-binding pocket and the principal quaternary ammonium-binding site. However, the tertiary amine group of galanthamine does not directly interact with Trp84. A docking study using the program AUTODOCK correctly predicts the orientation of galanthamine in the active site. The docked lowest-energy structure has a root mean square deviation of 0.5Å with respect to the corresponding crystal structure of the complex. The observed binding mode explains the affinities of a series of structural analogs of galanthamine and provides a rational basis for structure-based drug design of synthetic derivatives with improved pharmacological properties. Proteins 2001;42:182–191.**

Key words: Alzheimer's disease; cholinesterase inhibitors; drug design; protein crystallography

INTRODUCTION

Alzheimer's disease (AD) is a neurodegenerative disorder of the central nervous system that is characterized by profound memory impairment, emotional disturbance, and, in late stages, by personality changes. Studies of brain tissue indicate that neural loss, synaptic damage, and increased levels of neurofibrillary tangles, neuritic plaques, and granulovacuolar degeneration accompany AD.[1] At the molecular level, the major components of the tangles and plaques have been identified, and it has been found that AD is associated with reduced levels of choline acetyltransferase, acetylcholinesterase (AChE), and nicotinic acetylcholine receptors (nAChR).[2] Overall, this results in a dramatic dysfunction of the central cholinergic system. The cholinergic approach to the treatment of AD is aimed at the reactivation of the functionality of this system, with consequent reduction of the severity of the symptoms.[3]

The rationale behind most of the current drug therapeutic approaches to AD is the elevation of the transient levels of acetylcholine (ACh) in the brain or a direct enhancement of nicotinic receptor activation by the application of cholinesterase inhibitors or nicotinic agonists, respectively.

The only two drugs approved by the United States Food and Drug Administration (FDA) for the treatment of AD are both reversible inhibitors of AChE. They are tacrine, marketed as Cognex,®[4] and, recently, the more potent E2020, marketed as Aricept®.[5] However, both have drawbacks such as hepatotoxicity and, in the case of tacrine, low selectivity for AChE vs. butyrylcholinesterase (BChE); this may be important, as it has been suggested that inhibition of BChE, which is abundant in human plasma, may cause increased side effects.

Galanthamine (Fig. 1), a tertiary alkaloid extracted from several species of *Amaryllidacae*, has received recent attention as a centrally acting, selective, competitive, and reversible cholinesterase inhibitor that produces significant improvement of cognitive performances in AD patients. Although galanthamine has been used in the past

Abbreviations: AChE: Acetylcholinesterase; AD: Alzheimer's Disease; Tc: *Torpedo californica.*

Crystallographic co-ordinates and observed structure factors have been deposited at the Brookhaven Protein Data Bank (accession codes 1qti and r1qtisf).

*Correspondence to: Doriano Lamba, International Centre for Genetic Engineering and Biotechnology, Area Science Park, Padriciano 99, I-34012 Trieste, Italy. E-mail: lamba@sci.area.trieste.it or lamba@icgeb.trieste.it

Received 10 April 2000; Accepted 15 September 2000

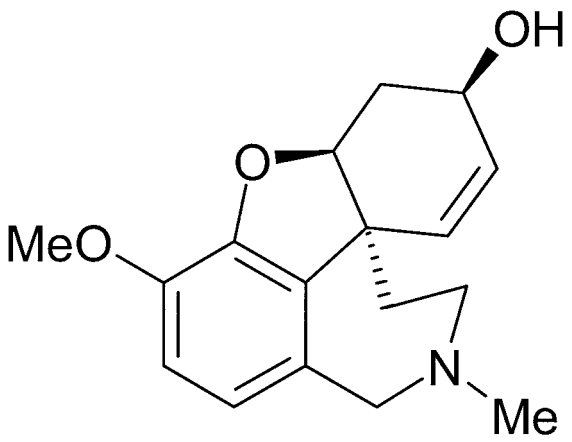

Fig. 1. Chemical structure of (-)-galanthamine.

for the treatment of a variety of neurological disorders, nowadays it attracts attention as a possible agent in the treatment of AD. This compound is less potent than tacrine and E2020 but has excellent pharmacological and pharmacokinetic profiles and it exhibits very low hepatotoxicity and side effects.[6–8] Nivalin® (Galanthamine hydrobromide) is in the final stages of clinical evaluation and has recently received its first approval for the treatment of AD in Austria and in Sweden. The cost of obtaining galanthamine from natural sources is very high, and a total synthesis procedure via (−)-narwedine has been extensively worked out for large-scale industrial preparation.[9]

Recently a novel class of nAChR ligands has been described, acting as allosterically potentiating ligands on the nicotinic responses induced by ACh and competitive agonists.[10] Galanthamine is a representative member of this class of ligands, and its action is exerted via a binding site on nAChR that is distinct from the site for acetylcholine. Therefore, galanthamine acts as a noncompetitive nicotinic receptor agonist. Since there is much evidence indicating that neural nAChR receptors play an important role in learning and memory, the fact that nicotinic agonists upregulate neuronal nAChR can be used in the development of new drugs for the treatment of AD.[3] Galanthamine together with physostigmine is among the very few drugs that exhibit a dual activity, acting not only as an inhibitor of AChE but also as an allosteric potentiator of the nicotinic response induced by ACh and competitive agonists.[10]

During the past years, many galanthamine derivatives have been synthesized and tested for their activities as drugs for the treatment of AD.[11] Recently, the 3D crystal structures of a number of AChE–inhibitor complexes have been determined.[12–17] The results of structural analyses of complexes of drugs and their target proteins may lead to design new agents with improved pharmacological properties. The ability to accurately predict the bound conformation of new lead compounds is a prerequisite for structure-based drug design to be successful and X-ray crystallography has proven to be an invaluable tool for making a correct protein–ligand structural assignment.[12,15] In the case of galanthamine, docking protocols suggest more than one orientation.[18,19] The 3D crystal structure determination of an AChE–galanthamine complex would permit unequivocal resolution of this issue. Furthermore, it would provide a rational basis for structure-related drug design aimed at developing synthetic analogs of galanthamine with improved pharmacokinetic and pharmacodynamic properties.

We now report the 2.5Å crystal structure of this complex, which permitted us to determine the correct orientation and interactions of galanthamine within the active-site gorge.

MATERIALS AND METHODS

Crystallization

Sanochemia Pharmazeutika AG (Wien, Austria) kindly provided Galanthamine. *Torpedo californica* AChE (*Tc*AChE) was extracted, purified, and crystallized as previously described.[20] Crystals grew in 2–3 weeks up to a size of $150 \times 150 \times 200\ \mu m^3$. The crystals of the *Tc*AChE–galanthamine complex were obtained by soaking the native crystals at 4°C in 10 mM galanthamine, 42% PEG200, 100 mM MES at pH 6.0, for 3 days.

Structure Determination

X-ray diffraction data were collected with a Mar345 imaging plate (X-ray Research, Hamburg, Germany) at the XRD1 beam line of the Italian Synchrotron facility ELETTRA (Trieste, Italy). The crystals were flash-cooled at 120K, using an Oxford Cryosystems cooling device (Oxford, UK), by being transferred directly from the soaking solution to a stream of boiled-off nitrogen. Data processing was done with DENZO, SCALEPACK,[21] and the CCP4 package.[22] The refined coordinates of the native *Tc*AChE,[12] PDB accession code 2ace,[23] were used after removal of the water molecules to calculate the initial phases for the enzyme–inhibitor structure. The structure was determined by the difference Fourier technique. The X-PLOR[24] program was used for crystallographic refinement. For the complex ($2F_o$-F_c) and (F_o-F_c) maps were computed after initial refinement of the native protein by simulated annealing (at a maximum temperature of 3,000 K), followed by conjugate gradient minimization and restrained individual atomic temperature factor refinement. A prominent difference electron density feature in the catalytic gorge allowed unambiguous fitting of the galanthamine moiety. The model used for galanthamine was taken from the coordinates of the X-ray crystal structure of the free base.[25] Peaks in the difference Fourier maps that were greater than 2.5σ and that displayed good hydrogen-bonding geometry to the protein were built in as solvent molecules. Map inspection and model correction during refinement were based on the graphics program O.[26] In the last few refinement cycles, very weak reflections with a ratio F_{calc}/F_{obs} greater than 2.5, clearly affected by systematic measurements errors, were excluded from the calculations. Statistics of crystallographic analysis and refinement are shown in Table I.

TABLE I. Crystal, Data Collection, and Refinement Statistics of the *Tc*AChE-Galanthamine Complex[†]

Crystal parameters	
Space group	$P3_121$
Cell constants	$a = b = 110.82, c = 136.45$ Å $\alpha = \beta = 90°, \gamma = 120°$
Data collection	
X-ray source	XRD1, ELETTRA, Trieste (Italy)
Wavelength, Å	1.00
Temperature, K	120.0
Resolution range, Å	20.0–2.3 (2.4–2.3)
Measurements	188,745
Unique reflections $I \geq 0\sigma(I)$	42,574 (5,493)
Completeness, %	96.1 (85.9)
Multiplicity	4.4 (2.8)
R_{sym} %	7.1 (21.0)
Mean $I/\sigma(I)$ of merged data	7.7 (3.4)
Refinement statistics	
Resolution used, Å	8.0–2.5
Reflections used $F_o \geq 2\sigma(F_o)$	27,322
R_{cryst}, R_{free} %	19.2, 23.6
R.m.s.d. on bond lengths, Å [a]	0.006
R.m.s.d. on bond angles, ° [a]	1.2
Number of atoms	
Protein	4,167
Water	172
Inhibitor	21
All atoms	4,360
Average temp. Factors, Å^2	
Protein	32.7
Water	46.2
Inhibitor	29.6
All atoms	33.2
R.m.s.d. ΔB, Å^2 [b]	3.30

[†]Numbers in parentheses refer to the shell of highest resolution data. $R_{sym}(I) = \Sigma_{hkl} \Sigma_i |I_{hkl,i} - \langle I_{hkl} \rangle| / \Sigma_{hkl} \Sigma_i |I_{hkl,i}|$ with $\langle I_{hkl} \rangle$ mean intensity of the multiple $I_{hkl,i}$ observations from symmetry-related reflections. $R_{cryst} = \Sigma_{hkl} |F_o - F_c| / \Sigma_{hkl} F_o$ where F_o and F_c are the observed and calculated structure factor amplitudes for reflection hkl. The R_{free} was calculated by randomly omitting 5% of the observed reflections from the data set.

[a]Stereo-chemical criteria are those of Engh and Huber.[27]

[b]R.m.s.d. ΔB is the r.m.s. deviation of the B factor of bonded atoms.

Docking

Parallel to the elucidation of the crystal structure we investigated the *Tc*AChE–galanthamine complex by molecular modeling techniques. We have employed the automated docking procedure as implemented in the program AUTODOCK 2.4[28] using a box of $22.5 \times 22.5 \times 22.5$Å^3 to include 42 amino acids delimiting the active site gorge. The size of the box was deliberately chosen fairly large in order to allow ligand binding in the whole catalytic pocket, which extends about 20Å from the peripheral anionic site at the top, in the region of Trp279, to the anionic site at the bottom, in the region of Trp84. A detailed description of the employed procedure has been reported elsewhere.[18]

The AUTODOCK package does not allow for the conformational flexibility of ring systems to be taken into account. Thus, the axial (ax) and equatorial (eq) orientation of the N-Methyl group in the tetrahydroazepine ring were considered independently in the computational study. The initial equatorial and axial conformations of the N-methyl group of galanthamine were taken from the crystal structures of the free base[25] and hydrobromide salt,[29] respectively.

A comparison of the crystal structures of the *Tc*AChE complexes showed that the side chain of Phe330 displays significant conformational flexibility, acting as a swinging gate.[15] The chosen side chain orientation of Phe330 was like the one observed in the *Tc*AChE–decamethonium[13] and *Tc*AChE–E2020[15] complexes, respectively.

Both eq- and ax-conformers of galanthamine were initially placed at or near the catalytic pocket. Then the AUTODOCK procedure was initiated and 500 runs were performed for each of the two conformers. As a result of the comparatively large active site box, in a significant number of runs galanthamine was found to be placed at the peripheral anionic site rather than inside or at the bottom of the gorge. After the simulations, as many as 57 (eq)- and 22 (ax)- galanthamine conformers resided inside the gorge. Because of the established competitive binding behavior of galanthamine, only these structures were considered and were ranked, on energy values of the *Tc*AChE–galanthamine complexes, by AUTODOCK into 6 clusters for the galanthamine (eq)-conformer and 4 for the (ax)-conformer, respectively. The energy model adopted in AUTODOCK includes both Van der Waals and electrostatic potentials with parameters based on the AMBER force field.[30] A dielectric constant distance dependent function is used to approximate the charge-charge interactions. One representative of each of the resulting 10 clusters from the AUTODOCK run was submitted to a geometry optimization within the electrostatic and steric fields of the enzyme's active site by using the TRIPOS force field (Pullman charges) as implemented in the SYBYL software (Version 6.5).[31] During this process, the subset of 42 amino acids employed in the docking studies was kept flexible to allow for an induced fit between the enzyme and the ligand. No unambiguous assignment can be made as to the preferred galanthamine structure, so that additional processes are necessary to determine the correct orientation and conformation of galanthamine in the *Tc*AChE binding site. The TRIPOS force field, however, can only provide an estimate of the enthalpic but not of the entropic contribution to the enzyme-inhibitor-free energy of binding. The resulting complexes were ranked according to the total energy of the AChE–ligand complex and the binding enthalpy of this complex, derived by subtracting the sum of the energies of the ligand and the enzyme in their free state from the energy of the ligand–enzyme complex.

RESULTS AND DISCUSSION

Overall Structure

The overall structure of the *Tc*AChE–galanthamine complex does not display significant conformational changes when compared to the structure of the free enzyme.[12] Contouring at 1.0σ level of the initial unbiased ($2F_o$-F_c) electron density map (Fig. 2) clearly shows the

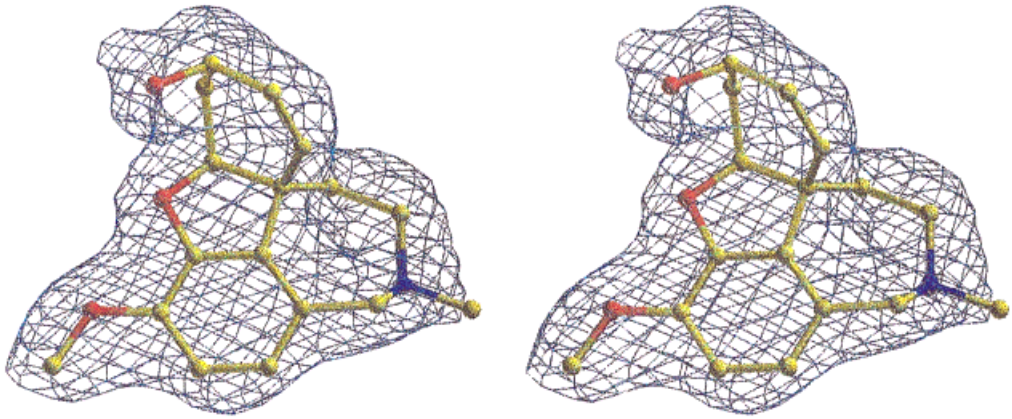

Fig. 2. Stereo view of the refined structure of galanthamine (ball and stick model) in the active site of *Tc*AChE displayed in the initial $2F_o$-F_c map with 1.0σ cut-off, showing the excellent fit of the molecule to the electron density (the picture was generated with O[26]).

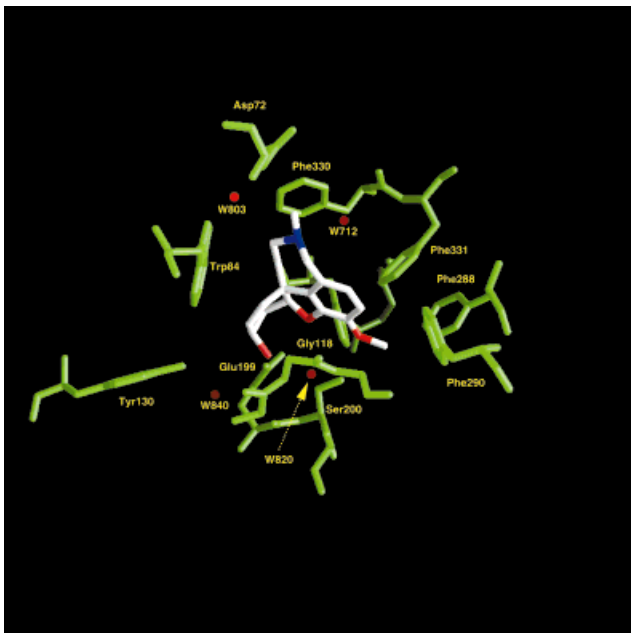

Fig. 3. Perspective view of the binding of galanthamine in the active site gorge of *Tc*AChE. Selected protein residues are shown as sticks models in green. Water molecules are red spheres (picture made with GRASP[32]).

shape of the galanthamine molecule at its location at the bottom of the active site gorge. The seven-membered tetrahydroazepine ring is in a chair conformation with the N-methyl group in an equatorial orientation. The configuration of the N-atom is the same as observed in the crystal structure of the free base.[25] An axial N-methyl configuration, probably as a result of stereoelectronic effects, is found in the crystal structure of the hydrobromide salt.[29] The inhibitor binds at the base of the gorge, occupying the acyl binding pocket and the binding site for quaternary ligands near Trp84, respectively. The mode of binding of galanthamine to *Tc*AChE is shown in Figure 3.

Protein–Ligand Interactions

The principal protein–ligand interactions revealed by the refined structure include:

1. The hydroxyl oxygen of the inhibitor forms a strong hydrogen bond with the charged Glu199-$O^{\epsilon 1}$ (2.7Å). The hydroxyl moiety also interacts with two water molecules. The first water molecule, W820 (B = 25.5Å^2), is 2.7Å apart from the hydroxyl group of the inhibitor. This water molecule is firmly bound in the catalytic pocket by the Ser200-O^{γ} (2.7Å), by three NH groups of the "oxyanion hole" lined by residues Gly118 (2.5Å), Gly119 (3.2Å), and Ala201 (3.1Å), and it is also involved in hydrogen bonding with the oxygen of the dihydrofuran ring of the inhibitor (3.1Å). The second water molecule, W840 (B = 34.4Å^2), is 3.5Å away from the hydroxyl group of the inhibitor and interacts also with Tyr130-O^{η} (2.5Å) and Gly117-N (2.8Å). It is noteworthy that the pattern of interactions of the water molecule W840 in the *Tc*AChE–galanthamine complex is conserved in the native AChE and in all other inhibitor complexes.[33] This may be relevant in structure-based drug design and in molecular dynamics simulations. The water molecules W820 and W840, as well as W712, W717, and W803 (see below) have strikingly low B-values, lower than the average B value for all the protein atoms (B = 33.2Å^2). Thus, these water molecules have very well-defined positions.
2. The cyclohexene ring and two methylene groups (C11 and C12) in the tetrahydroazepine ring of galanthamine face towards the indole ring of Trp84. The double bond (C1═C2) in the cyclohexene ring stacks against the π system of the indole ring forming a favorable π–π interaction, the closest contacts being between C2 and Trp84-$C^{\epsilon 3}$ (3.5Å) and between C(11) and Trp84-$C^{\delta 1}$ (3.8Å), respectively.
3. The methyl moiety of the methoxy group of galanthamine occupies the acyl-binding pocket and its orientation is stabilized by non-bonded σ–π interactions involving residues Phe288-$C^{\epsilon 1}$ (3.2Å), Phe290-C^{ζ} (3.5Å),

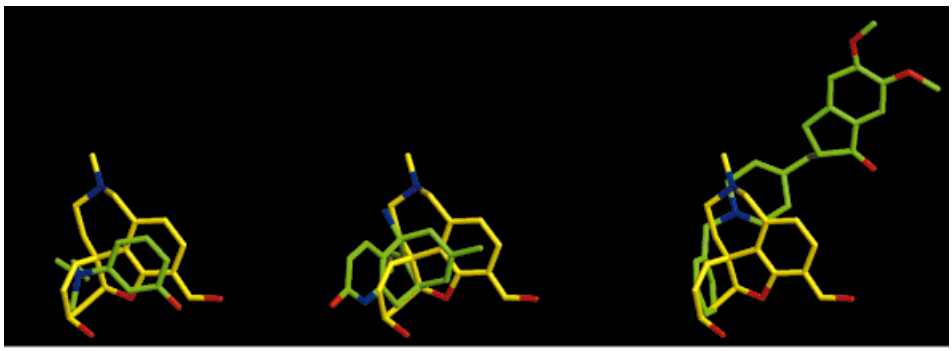

Fig. 4. Overlay of *Tc*AChE-galanthamine complex and *Tc*AChE-edrophonium (**A**), *Tc*AChE-hyperzine A (**B**) and *Tc*AChE-E2020 (**C**) complexes respectively. For clarity the protein residues have been omitted. The inhibitors are displayed as stick models, with yellow (galanthamine) and green (edrophonium, huperzine A and E2020) carbon atoms respectively (picture made with WebLab ViewerPro™[39]).

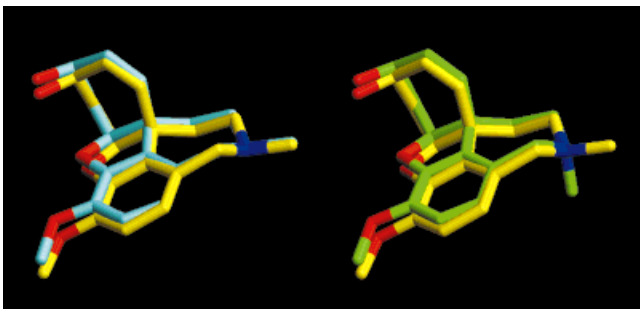

Fig. 5. Structural overlay of galanthamine structures as revealed by the modeling study with *Tc*AChE (eq-conformer in cyan and ax-conformer in green) and the corresponding crystal structure (yellow). (Picture made with WebLab ViewerPro™[39]).

and Phe331-C^{ζ} (3.7Å), respectively. The oxygen atom of the O-methyl group participates in hydrogen bonding with both the catalytic residue Ser200-O^{γ} (3.0Å) and the water molecule W820 (3.3Å).

4. The pKa of galanthamine is 8.32.[34] Hence at pH 6.0 (see Crystallization), the N-methyl group of the tetrahydroazepine ring is protonated, enabling a non-classical hydrogen bond interaction with both Asp72-$O^{\delta 2}$ (3.6Å) and the structurally conserved water molecule W803 (B = 29.9Å^2, 3.2Å).[33] The tertiary amine N interacts with the water molecule W712 (B = 26.8Å^2, 3.3Å), which in turn forms an aromatic hydrogen bond with Phe330 (3.7Å).[35] This water molecule fulfills the same role as the terminal hydroxyl group of the PEG molecule present in the crystal structure of the *Tc*AChE–galanthamine complex determined independently by Greenblatt et al.[19] Surprisingly, the protonated tertiary amine group does not directly interact with the anionic sub site near Trp84 as observed in the AChE complexes with huperzine A,[12] tacrine,[13] edrophonium,[14] decamethonium,[13] and μ-(N, N′, N″-trimethylammonium) trifluoroacetophenone.[16] The distance from the tertiary amine N to the centroid of the indole moiety of Trp84 is 6.2Å. Furthermore, no interaction occurs with the proposed additional quaternary ion binding site, Phe330, lining midway down the gorge, as observed in the AChE complex with E2020.[15] The distance from the tertiary amine N to the centroid of the phenyl moiety of Phe330 is 5.2Å. However, Phe330 adopts the same orientation in both the galanthamine and the E2020 AChE complexes. This residue, which assumes a wide range of conformations, is called the "swinging gate" and it has been suggested that it may act, via a shuttle-like mechanism, as a gate for the molecular trafficking to and from the active site.[15,36] Interestingly, recent molecular modeling, dynamics simulations, and kinetic studies have also pointed out the contribution of Asp72 to the specificity and catalytic activity of cholinesterases. Asp72 may act as an electrostatic anchor that traps cationic ligands entering the active site gorge.[36–38]

Comparison of the *Tc*AChE–Galanthamine Complex With Other *Tc*AChE–Inhibitor Complexes

The structures of the native *Tc*AChE and of 9 different complexes were superimposed according to their C^{α} positions, namely native AChE (PDB code 2ACE),[12] and the complexes with the physostigmine analog MF268 (PDB code 1OCE),[17] E2020 (PDB code 1EVE),[15] huperzine A (PDB code 1VOT),[12] tacrine (PDB code 1ACJ),[13] edrophonium (PDB code 2ACK),[14] decamethonium (PDB code 1ACL),[13] μ-(N, N′, N″-trimethylammonium) trifluoroacetophenone (PDB code 1AMN),[16] galanthamine (PDB code 1DX6 and 1QTI) (Greenblatt et al.[19] and present work).

It would have been predicted for galanthamine to share with competitive inhibitors a common binding area at the bottom of the gorge. Overall, the crystal structures of the complexes reveal that the inhibitors have unique, largely non-overlapping binding orientations in the active site of the enzyme. Nonetheless, the overlay of the *Tc*AChE–galanthamine complex with the complexes of *Tc*AChE–edrophonium, *Tc*AChE–huperzine A, and *Tc*AChE–E2020, respectively (Fig. 4) highlights some common structural features among these inhibitors, as follows:

TABLE II. Comparison of the Resulting Structures for Galanthamine and Derivative 5, Respectively, from Modeling Studies Bearing the (eq)- and (ax)-Configurations[†]

Structure	Cluster no.	r.m.s.d. [Å]	Energy of the complex [kcal/mol]	Binding enthalpy [kcal/mol]
Galanthamine (equatorial)	eq26	0.58	−4002.6	−61.5
	eq01	2.07	−4001.1	−57.8
	eq03	3.29	−3991.0	−46.0
	eq27	3.14	−3984.4	−44.2
	eq04	3.69	−3983.7	−40.8
	eq02	3.49	−3981.1	−37.3
Galanthamine (axial)	ax24	0.46	−4003.5	−60.1
	ax01	2.20	3990.0	−44.1
	ax02	2.22	3983.7	−41.7
	ax16	3.89	3980.7	−35.5
Structure	Cluster no.	r.m.s.d. (core) [Å]	Energy of the complex [kcal/mol]	Binding enthalpy [kcal/mol]
5 (equatorial)	eq18	0.41	−4010.6	−75.2
	eq37	0.40	−4006.6	−73.2
5 (axial)	ax25	0.50	−4010.2	−76.3
	ax22	0.56	−4006.8	−74.4

[†]R.m.s.d. values (Å) denote the deviations from the orientation observed in the x-ray crystal structure of the *Tc*AChE-galanthamine complex. The r.m.s.d. (core) (Å) values reflect the deviations of the ring structure of derivative **5** from that observed in the x-ray crystal structure of the complex. The binding enthalpies of the complexes are derived by subtracting the sum of the energies of the ligand and of the enzyme in their free state from the energy of the ligand-enzyme complex.

1. The benzene rings of galanthamine and edrophonium, are oriented almost parallel to each other, with an angle of 20°, and are displaced by an average distance of 1.1Å (range 1.0–1.3Å). The oxygen atoms belonging to the methoxy group of galanthamine and to the hydroxyl group of edrophonium, respectively, are 0.8Å apart while the protonated nitrogen atoms are 4.2Å away (Fig. 4, **A**).
2. The water molecule W717 (B = 23.0Å^2) observed in the *Tc*AChE–galanthamine complex interacts with Tyr130-O$^{\eta}$ (2.9Å) and the oxygen of the carbonyl group of Gly117-O (2.8Å). This solvent molecule is conserved in all complexes that have been determined so far but in the huperzine A complex,[33] where it is displaced by the pyridone oxygen of the ligand that interacts with Tyr130-O$^{\eta}$ (2.6Å) but no longer with the carbonyl oxygen of Gly117. Indeed, the peptide bond between Gly117 and Gly118, in the "oxyanion hole," exhibits a major conformational change that accounts for the binding of huperzine A. The tertiary ammonium group of galanthamine is 1.8Å away from the primary ammonium group of huperzine A (Fig. 4, **B**).
3. The cyclohexadiene and phenyl rings of galanthamine and E2020, respectively, are 35° off one another, and are displaced by an average distance of 0.7Å (range 0.3–1.3Å). The protonated nitrogen atom of the tetrahydroazepine ring of galanthamine and the equivalent nitrogen of the piperidine ring of E2020 are 1.6Å apart (Fig. 4, **C**).

Comparison of the Docking Models With the X-Ray Structure of the *Tc*AChE–Galanthamine Complex

The automated docking procedure revealed that the galanthamine models "eq26" and "ax24" (see Table II) have the most likely orientation of the ligand within the active site gorge of *Tc*AChE. In order to evaluate how well the predicted orientations of galanthamine compare with that found in the present crystal structure, the polypeptide backbones of each of the SYBYL energy minimized models were superimposed on the X-ray structure of the complex by a rigid RMS fit routine. The RMS deviations of the various predicted orientations of galanthamine from that of the crystal structure are reported in Table II. Remarkably, the galanthamine highest scoring models, "eq26" and "ax24", also proved to be those having by far the lowest RMS deviations from the X-ray crystal structure, 0.58Å and 0.46Å respectively (Fig. 5). Indeed, both conformers give excellent RMS values despite the different orientation of the N-methyl group in the structures. However, the modeling procedure is not able to assign the axial or the equatorial conformation as the preferred orientation. Docking studies on galanthamine derivatives with longer alkyl chains at the nitrogen atom might help to resolve this issue and to establish whether extended binding may occur via favorable interactions with a number of residues in the gorge. For this purpose, we modeled the *Tc*AChE complex with the galanthamine derivative **5** (see Fig. 6). The orientation and conformation of this analog was predicted using the same procedure described for galanthamine itself and indeed **5** showed the expected extension of the N-alkyl chain towards the peripheral anionic site. However, the equatorial "eq18" and the axial "ax25" conformer show nearly identical binding enthalpy. Both highest scoring models of **5** (see Table II) have been superimposed on the crystal structures of decamethonium,[13] E2020,[15] and MF268,[17] which are known to bind with an extended conformation along the active site gorge (see Fig. 7).

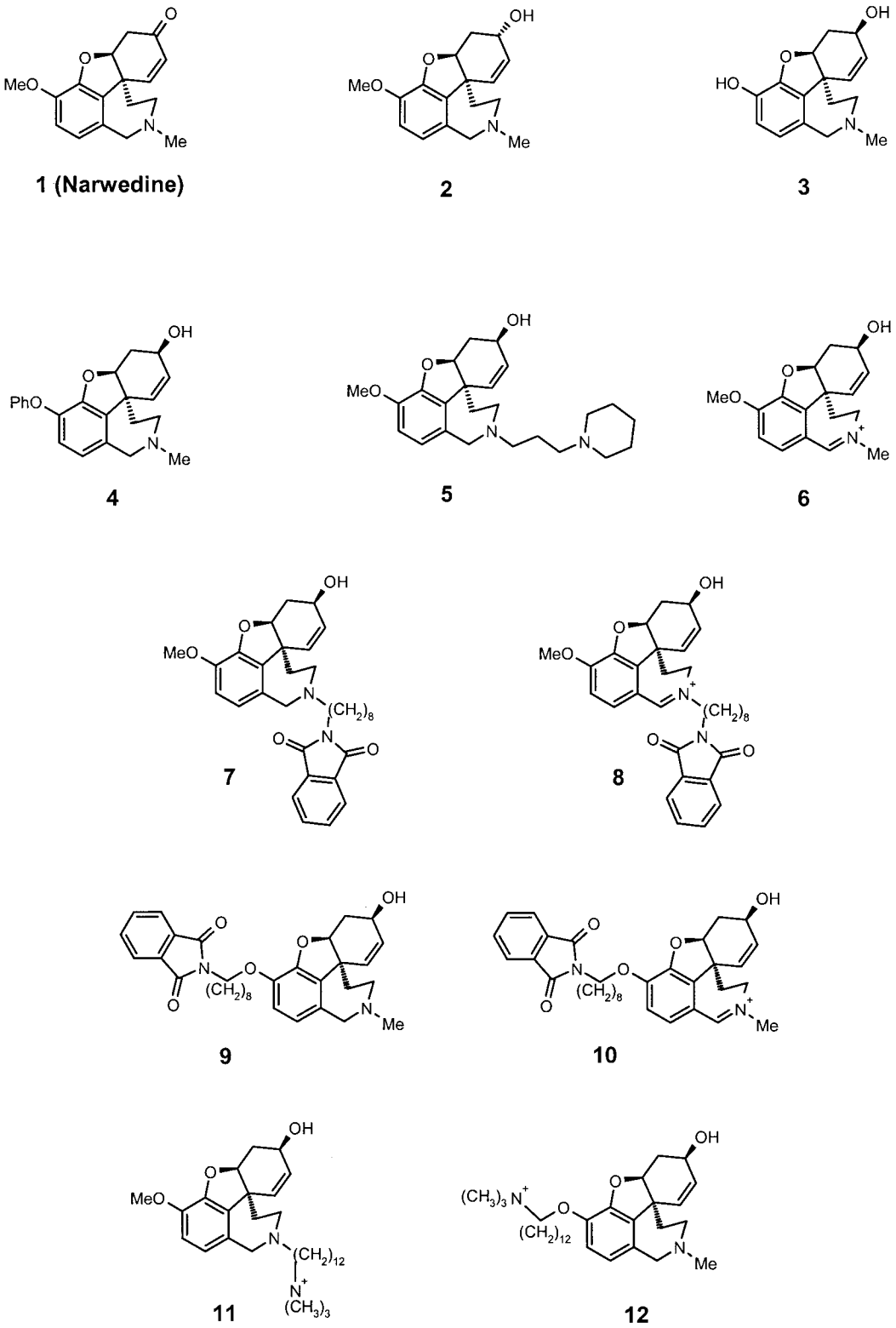

Fig. 6. Chemical structures of galanthamine analogs.

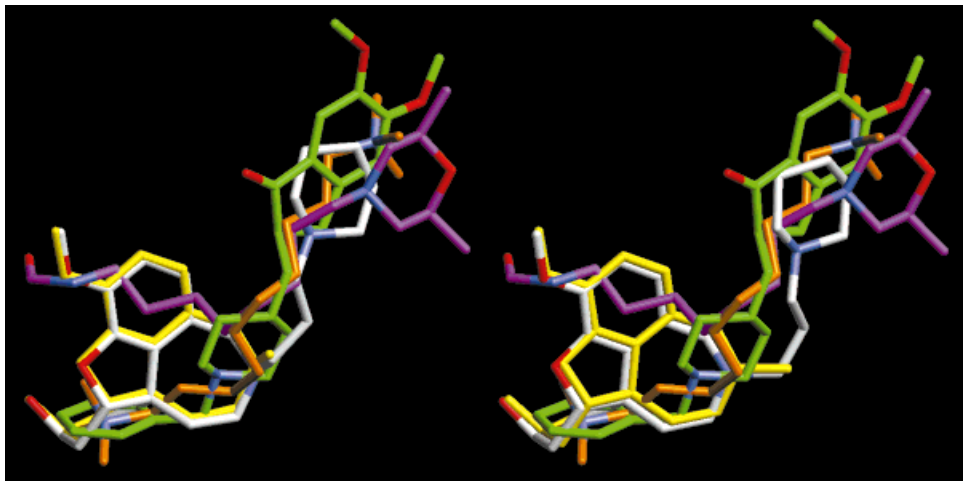

Fig. 7. Structural overlay of the highest scoring (ax)-conformer (left) and (eq)-conformer (right) of galanthamine derivative **5** (white) with the corresponding galanthamine (ax)-conformer and (eq)-conformer as revealed by the modeling study (yellow). For comparison the crystal stuctures of decamethonium (1ACL, brown), E2020 (1EVE, green) and MF268 (1OCE, pink) are shown (picutre made with WebLab ViewerPro™[39]).

TABLE III. In Vitro Electrophorus Electricus-AChE Inhibition

Compound	IC_{50} (μM)	Ref.
Galanthamine	0.36	40,41
1 (Narwedine)	30.0	40
2	30.0	40
3	0.03	40
4	3.15	40
5	0.03	40
6	0.14	41
7	0.28	41
8	0.01	41
9	2.50	41
10	0.07	41
11	0.08	41
12	1.30	41

Structure–Activity Relationships of Galanthamine Analogs

The crystal structure of the *Tc*AChE–galanthamine complex shows an unexpected orientation within the active-site gorge and a surprisingly few strong direct interactions of the inhibitor with protein residues to explain its affinity (Table III). The analysis of the complex allows the rationalization of the reported differences in affinity of the structural analogs of galanthamine for *Electrophorus electricus* AChE.[40,41]

Modifications of the Hydroxyl Function and of the Cyclohexene Ring

The oxidation of the hydroxyl, compound **1**,[40] or the inversion of its configuration, compound **2**,[40] result in a drastic decrease of activity, since both modifications disrupt the strong hydrogen bond interaction with the carboxylate moiety of Glu199. The saturation of the double bond in the cyclohexene ring to give lycoramine[42] does not allow a π–π interaction with Trp84 to occur and greatly reduces the binding affinity of the inhibitor.

Modifications of the Methoxyl Function

The demethylation of galanthamine increases the enzyme inhibitory activity.[40] Indeed, the higher affinity of compound **3** can be ascribed to the higher degree of polarization of the hydroxyl group, which is now involved in hydrogen bonding as acceptor with O^{γ} of Ser200 and as donor with $N^{\epsilon 2}$ of His440. On the contrary, the introduction of a benzyl group, compound **4**, brings a loss of activity.[40]

Mono-substituted N-alkylcarbamates of 6-demethylgalanthamine are very potent, although lethal, inhibitors of AChE.[11] The activity, however, is due to their acting as traditional carbamates, like the analogs of physostigmine,[43–45] whose mechanism of action is characterized by a fast carbamoylation of the catalytic serine followed by a slow regeneration of the active enzyme. The changes in activity within the carbamate series are probably modulated by the interactions of the alkyl chain with the hydrophobic residues lining the interior of the gorge.[17]

Modifications at the Tertiary Amine Site

With the aim of synthesizing derivatives potentially capable of bridging the anionic subsite at the bottom and the peripheral anionic site at the top of the catalytic gorge, an N-alkyl chain analog of galanthamine has been prepared. Indeed, compound **5**[40] showed an encouraging increase in activity that can be rationalized on a structural basis, the tetrahydroazepine ring of galanthamine being oriented up the gorge. Our molecular modeling and docking studies, however, revealed the alkyl spacer to be too short to allow an optimal interaction between Trp279 and the piperidine moiety.[18]

Several other bis-interacting ligands, compounds **7–12**, have been prepared and studied by Mary et al.[41] For the preparation of such ligands, via alkyl spacers of varying

lengths, both the tertiary amine moiety and the methoxy function, have been exploited. N-substituted phthalimido compound **7** shows an inhibitory activity comparable to galanthamine, whereas N-alkylammonium compound **11** is more potent. The O-bis interacting compounds **9** and **12** show reduced affinity with respect to galanthamine and the N-bis-interacting derivatives **7** and **11**. In fact, any bulky modification of the methoxy group, which faces the bottom of the gorge and has a hindered accessibility, would force a rearrangement of galanthamine within the catalytic pocket and thus weaken the interactions with the neighboring side chains of the protein residues. Mary et al.[41] further noticed that the introduction of an iminium function, compounds **6**, **8**, and **10** greatly enhances the inhibitory activity. Indeed, this permanent positive charge on the galanthamine nitrogen atom constitutes the major factor in determining AChE inhibition potency since for compound **10**, the less favorable linkage to the oxygen atom is largely offset by the presence of the iminium function. In the *Tc*AChE–E2020 complex,[15] the charged nitrogen of the piperidine ring makes a cation–π interaction[46] with the phenyl ring of Phe330. Kryger et al.[15] suggested that Phe330 might serve as an additional quaternary binding site midway down the gorge. However, the structure of the *Tc*AChE–galanthamine complex highlights the fact that the protonated nitrogen of galanthamine (crystals were grown at pH 6.0) is located far from the anionic sub site, near Trp84, and it shows only a weak interaction through the water molecule W712 with Phe330. Hence, the reasons for the iminium derivatives **6**, **8**, and **10** to be better AChE inhibitors are unclear. One possible explanation is based on the assumption that the planar geometry of the nitrogen atom would allow the N-methyl group to better interact with the carboxylate of Asp72.

CONCLUSIONS

The crystal structure analysis of the *Tc*AChE–galanthamine complex reveals an unexpected orientation of the ligand within the active site, as well as unusual protein–ligand interactions: (1) the protonated tertiary amine does not closely interact with Trp84; (2) one of the direct hydrogen bonds with the protein involves the charged residue Glu199; and (3) it also binds in the acyl-binding pocket. Overall, these structural details provide a rational basis for structure-based drug design aimed at developing synthetic analogs of galanthamine with improved therapeutic properties, with high affinity for AChE and a high degree of selectivity for AChE vs. BChE. Recent studies suggest that the differential specificity for AChE and BChE can be attributed to structural differences at the peripheral anionic site[15] rather than differences in the geometry within the active site.[47] Avoiding the inhibition of BChE is an important clinical consideration due to the likely potentiating side effects. In this context it is worth noting that the 3D structure of *Torpedo californica* AChE is very similar to those of both mouse[48] and human[49] AChE. Thus, the conclusions drawn from the structure of the *Tc*AChE–galanthamine complex should be valid for the mammalian enzyme.

ACKNOWLEDGMENTS

We gratefully acknowledge Dr. J. Roither and Dr. K. Czollner (Sanochemia Pharmazeutika AG, Wien, Austria) for generously providing us with galanthamine and, prior to publication, with activity data on some of the galanthamine analogs reported in Table III.

REFERENCES

1. Hardy JA, Higgins GA. Alzheimer's disease: the amyloid cascade hypothesis. Science 1992;256;184–185.
2. Selkoe DJ. Biochemistry of altered brain proteins in Alzheimer's disease. Annu Rev Neurosci 1989;12:463–490.
3. Maelicke A, Albuquerque EX. New approach to drug therapy in Alzheimer's dementia. DDT 1996;1:53–59, and references cited therein.
4. Davis KL, Powchik P. Tacrine. Lancet 1995;345:625–630.
5. Kawakami Y, Inoue A, Kawai T, Wakita M, Sugimoto H, Hopfinger AJ. The rationale for E2020 as a potent acetylcholinesterase inhibitor. Bioorg Med Chem 1996;4:1429–1446.
6. Harvey AL. The pharmacology of galanthamine and its analogues. Pharmacol Ther 1995;68:113–128.
7. Raskind MA, Peskind ER, Wessel T, Yuan W. Galantamine in AD: A 6-month randomized, placebo-controlled trial with a 6-month extension. The Galantamine USA-1 Study Group. Neurology 2000;54:2261–2268.
8. Tariot PN, Solomon PR, Morris JC, Kershaw P, Lilienfeld S, Ding C. A 5-month, randomized, placebo-controlled trial of galantamine in AD. The Galantamine USA-10 Study Group. Neurology 2000;54:2269–2276.
9. Kuenburg B, Czollner L, Fröhlich J, Jordis U. Development of a pilot scale process for the anti-Alzheimer drug (-)-galanthamine using large scale phenolic oxidative coupling and crystallization-induced chiral conversion. Org Process Res Dev 1999;3:425–431.
10. Maelicke A, Schrattenholz A, Samochocki M, Radina M, Albuquerque EX. Allosterically potentiating ligands of nicotinic receptors as a treatment strategy for Alzheimer's disease. Behav Brain Res 2000;113:199–206, and ref. cit. therein.
11. Bores GM, Kosley RW JR. Galanthamine derivatives for the treatment of Alzheimer's disease. Drugs Future 1996;21:621–635.
12. Raves ML, Harel M, Pang YP, Silman I, Kozikowski AP, Sussmann JL. Structure of acetylcholinesterase complexed with the nootropic alkaloid, (-)-huperzine A. Nature Struct Biol 1997;4:57–63.
13. Harel M, Schalk I, Ehret-Sabatier L, Bouet F, Goeldner M, Hirth C, Axelsen PH, Silman I, Sussmann, JL. Quaternary ligand binding to aromatic residues in the active-site gorge of acetylcholinesterase. Proc Natl Acad Sci USA 1993;90:9031–9035.
14. Ravelli RBG, Raves ML, Ren Z, Bourgeois D, Roth M, Kroon J, Silman I, Sussman JL. Static Laue diffraction studies on acetylcholinesterase. (1998) Acta Crystallogr 1998;D54:1359–1366.
15. Kryger G, Silman I, Sussmann JL. Structure of acetylcholinesterase complexed with E2020 (Aricept®): implications for the design of new anti-Alzheimer drugs. Structure 1999;7:297–307.
16. Harel M, Quinn DM, Nair HK, Silman I, Sussman JL. The X-ray structure of a transition state analog complex reveals the molecular origins of the catalytic power and substrate specificity of acetylcholinesterase. J Am Chem Soc 1996;118:2340–2346.
17. Bartolucci C, Perola E, Cellai L, Brufani M, Lamba D. "Back door" opening implied by the crystal structure of carbamoylated acetylcholinesterase. Biochemistry 1999;38:5714–5719.
18. Pilger C, Bartolucci C, Lamba D, Tropsha A, Fels G. Accurate prediction of the bound conformation of galanthamine in the active site of *Torpedo californica* acetylcholinesterase using molecular docking. J Mol Graphics Modell 2000; in press.
19. Greenblatt HM, Kryger G, Lewis T, Silman I, Sussman JL. Structure of acetylcholinesterase complexed with (-)-galanthamine at 2.3 Å resolution. FEBS Lett 1999;463:321–326.
20. Sussmann JL, Harel M, Frolow F, Varon L, Toker L, Futerman AH, Silman I. Purification and crystallization of a dimeric form of acetylcholinesterase from *Torpedo californica* subsequent to solubilization with phosphatidylinositol-specific phospholipase C. J Mol Biol 1988;203:821–823.
21. Otwinowski Z, Minor W. Processing of X-ray diffraction data

collected in oscillation mode. Methods Enzymol 1997;276:307–326.
22. Collaborative Computational Project No.4. The CCP4 Suite: Programs for protein crystallography. Acta Crystallogr 1994;D50:760–763.
23. Berman HM, Westbrook J, Feng Z, Gilliland G, Bhat TN, Weissig H, Shindyalov LN, Bourne PE. The protein data bank. Nucleic Acids Res 2000;28;235–242.
24. Brünger AT. X-PLOR, Version 3.851. A system for X-ray crystallography and NMR. New York: Yale University Press; 1996.
25. Carroll P, Furst GT, Han SY, Joullié M. Spectroscopic studies of galanthamine and galanthamine methiodide. Bull Soc Chim Fr 1990;127:769–780.
26. Jones TA, Zhou JY, Cowan SW, Kjeldgaard M. Improved methods for building protein models in electron density maps and location of errors in these models. Acta Crystallogr 1991;A47:110–119.
27. Engh RA, Huber R. Accurate bond and angle parameters for X-ray protein structure refinement. Acta Crystallogr 1991;A47:392–400.
28. Goodsell DS, Olson AJ. Automated docking of substrates to proteins by simulated annealing. Proteins Struct Funct Genet 1990;8:195–202.
29. Peeters OM, Blaten NM, De Ranter CJ. (-)-Galanthaminium bromide. Acta Cryst 1997;C53:1284–1286.
30. Cornell, WD, Cieplak P, Bayly CI, Gould IR, Merz KM Jr, Ferguson DM, Spellmeyer DC, Fox T, Caldwell JW, Kollman PA. A second generation force field for the simulation of proteins and nucleic acids. J Am Chem Soc 1995;117:5179–5197.
31. SYBYL, Version 6.5. TRIPOS Associates, Inc., 1699 South Hanley Road, Suite 303, St. Louis, MO, 63144, USA.
32. Nicholls A, Bharadwaj R, Honig B. GRASP: graphical representation and analysis of surface properties. Biophys J 1993;64:A166.
33. Koellner G, Kryger G, Millard CB, Silman I, Sussman JL, Steiner T. Active-site gorge and buried water molecules in crystal structures of acetylcholinesterase from *Torpedo californica*. J Mol Biol 2000;296:713–735.
34. Mikhailova D, Yamboliev I. Pharmacokinetics of galanthamine hydrobromide (Nivalin) following single intravenous and oral administration in rats. Pharmacology 1986;32:301–306.
35. Levitt M, Perutz MF. Aromatic rings act as hydrogen bond acceptors. J Mol Biol 1988 ;201:751–754.
36. Botti SA, Felder CE, Lifson S, Sussman JL, Silman I. A modular treatment of molecular traffic through the active site of cholinesterase. Biophys J 1999;77:2430–2450.
37. Tara S, Elcock AH, Kirchhoff PD, Briggs JM, Radic Z, Taylor P, McCammon JA. Rapid binding of a cationic active site inhibitor to wilde type and mutant mouse acetylcholinesterase: Brownian dynamics simulation including diffusion in the active site gorge. Biopolymers 1998;46:465–474.
38. Mallender WD, Szegletes T, Rosenberry TL. Acetylthiocholine binds to Asp74 at the peripheral site of human acetylcholinesterase as the first step in the catalytic pathway. Biochemistry 2000;39:7753–7763.
39. WebLab ViewerPro™, Version 3.5. San Diego: Molecular Simulations Inc.
40. Czollner K, Sanochemia Pharmazeutika AG, Wien, Austria, unpublished results.
41. Mary A, Renko DZ, Guillou C, Thal C. Potent acetylcholinesterase inhibitors: design, synthesis, and structure-activity relationships of bis-interacting ligands in the galanthamine series. Bioorg Med Chem 1998;6:1835–1850.
42. Han SY, Sweeney JE, Bachman ES, Schweiger EJ, Forloni G, Coyle JT, Davis BM, Joullié MM. Chemical and pharmacological characterization of galanthamine, an acetylcholinesterase inhibitor, and its derivatives. A potential application in Alzheimer's disease?. Eur J Med Chem 1992;27:673–687.
43. Brufani M, Marta M, Pomponi M. Anticholinesterase activity of a new carbamate, heptylphysostigmine, in view of its use in patients with Alzheimer-type dementia. Eur J Biochem 1986; 157:115–120.
44. Alisi MA, Brufani M, Filocamo L, Gostoli G, Licandro E, Cesta MC, Lappa S, Marchesini D, Pagella P. Synthesis and structure-activity relationships of new acetylcholinesterase inhibitors: morpholinoalkylcarbamoyloxyeseroline derivatives. Bioorg Med Chem Lett 1995;5:2077–2080.
45. Perola E, Cellai L, Lamba D, Filocamo L, Brufani M. Long chain analogs of physostigmine as potential drugs for Alzheimer's disease: new insights into the mechanism of action in the inhibition of acetylcholinesterase. Biochim Biophys Acta 1997;1343:41–50.
46. Dougherty DA. Cation-π interactions in chemistry and biology: a new view of benzene, Phe, Tyr, and Trp. Science 1996;271:163–168.
47. Harel M, Sussman JL, Krejci E, Bon S, Chanal P, Massoulié J, Silman I. Conversion of acetylcholinesterase to butyrylcholinesterase: modeling and mutagenesis. Proc Natl Acad Sci 1992;89:10827–10831.
48. Bourne Y, Taylor P, Bougis PE, Marchot P. Crystal structure of mouse acetylcholinesterase. A peripheral site-occluding loop in a tetrameric assembly. J Biol Chem 1999;274:2963–2970.
49. Kryger G, Giles K, Toker L, Velan B, Lazar A, Kronman C, Barak D, Ariel N, Shafferman A, Silman I, Sussman JL. Crystal structures of native and E202Q mutant human acetylcholinesterase complexed with fasciculin-II. Acta Cryst 1999;A55 Suppl:288.